Acoustic Phenomena in a Demand Mode Piezoelectric Ink jet Printer

Bogdan V. Antohe and David B. Wallace

MicroFab Technologies, Inc., Plano, Texas

This article addresses acoustic wave propagation in a piezoelectric ink jet printer. Acoustic resonances limit the operating frequency of ink jet devices and influence the timings of the electrical drive signals. In this study, the resonant frequencies in a multichannel printhead are determined through feedback from the fluid to the piezoelectric structure using an electrical impedance analyzer. We also analyze the influence of channel length on resonant frequency. In addition, the effect of different boundary conditions on the acoustic resonance of the channels was observed. Because the channels walls are compliant, the propagation of acoustic pressure waves in them is slower than the speed of sound in the fluid, which is a fluid property. The electrical impedance measurements allow the determination of the effective speed of sound in the channel and the optimal timing for the driving electrical signal. During printhead operation, the drop velocity can be modified by changing the duration of the electrical pulse sent to the piezoelectric actuator. The timing that produces the maximum drop velocity can be also related to the effective speed of sound in the channel. Comparison of the two data sets show that a printhead channel has an acoustical behavior closer to an open–open pipe.

Journal of Imaging Science and Technology 46: 409–414 (2002)

Introduction

The printing industry has evolved dramatically in the last few years with an increasing demand for high throughput, reliable, and low cost printers. This trend was observed both for the industrial printers and for the office printers. The initial printers operated in continuous mode in which pressure is applied to the ink, thus producing a stream of fluid that emerges from the orifice. The jet breaks into droplets on its own,[1,2] but, in order to achieve a better control of the drops, a precisely (frequency) produced perturbation is applied to the fluid thus generating drops synchronized with the perturbation. Emerging drops are electrically charged and later on are deflected by an electric field to either the desired location on the paper or to a catcher that captures the undesired drops.[3,4] While the continuos drop generation has a simple operation principle and can generate drops at very high frequencies it has a major disadvantage in the charge/deflect system where large potentials are required. Also the charge/deflect mechanism requires the paper to be further away from the printer nozzles and thus reduces the placement accuracy of the ink drops on paper.

A more advantageous principle for printing is drop-on-demand (DOD) in which drops are generated only when needed. DOD printers use two main principles: (1) sudden heating of the ink produces a vapor bubble that forces the fluid through the orifice (bubble jet), and (2) sudden movement of the walls of the ink passage produces acoustic waves that propagate towards the orifice, where the drop is generated; in most cases the wall movement is produced by a piezoelectric element. The present work concentrates on a DOD printer using a piezoelectric actuator. Various types of such printers are known and differentiate from each other through the configuration of the ink channel, shape and position of the piezoelectric actuator, orifice plate configuration, reservoirs and ink supply systems, etc.. The operation of all such printers is dependent on the way the acoustic waves, produced by the “instantaneous” movement of the piezoelectric actuator, propagate in the fluid channels. Optimization of the printer performance, especially at high frequencies of operation, requires good understanding of the acoustic phenomena taking place in the print head.[5,6]

Print quality is directly related to the drop formation, and a high quality print requires a stable drop with no satellites (smaller drops trailing the main drop). The drop is formed as an integration of the fluid velocities at the orifice and is a function of both the fluid properties (surface tension and viscosity) and of the fluid flow at the orifice (a direct result of the orifice/nozzle configuration and the pressure waves reaching the orifice). Satellites can be produced by secondary reflections of the pressure (acoustic) waves propagating in the channel. These reflections are also the source of the variation of drop volume and velocity as a function of frequency. Thus, it is desirable for controlling the satellites, that the reflected acoustic waves are damped quickly; this can be done by adjusting the fluid properties and changing the geometry of the ink passage.

The piezoelectric element is actuated with an electrical signal. By adjusting the timings of the signal ap-

Original manuscript received May 7, 2002

plied to the piezoelectric actuator to match the acoustic propagation, a reduction of the signal amplitude (voltage) is achieved and consequently the power used by the printer is reduced. The correlation of the driving waveform and the timing of the acoustic propagation in the print head makes it possible to produce drops with smaller diameter than the orifice diameter (drop size modulation) and thus increase the print resolution for a fixed orifice diameter.[7]

All optimization activities above require the analysis of acoustical phenomena in the print head. This work studies the acoustics in a piezoelectric DOD printer based on a configuration developed by MicroFab Technologies, Inc., for Compaq Corporation.[8–10] The analysis includes the effective speed of sound in the ink channels, the influence of end effects on the channel acoustics, the correlation between optimum driving parameters, drop volume and velocity and the channel length.

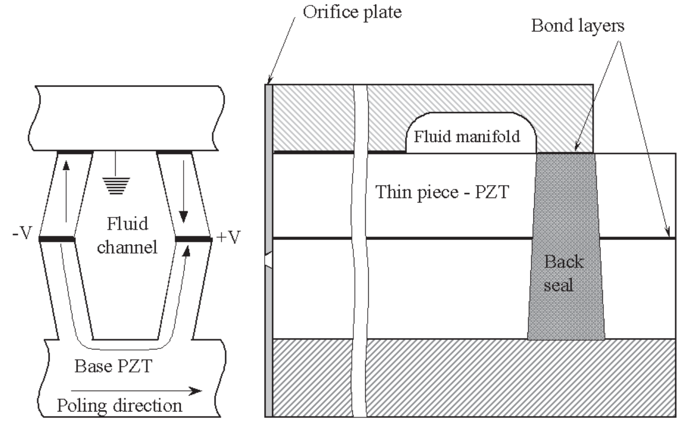

Figure 1. Printhead construction.

Theoretical Background

The propagation of the sound in elastic conduits does not take place with the intrinsic speed of sound (this happens only in infinite fluid reservoirs) but with a smaller speed due to the lateral compliance of the conduit walls. Wylie and Streeter[11] provide a relationship between the intrinsic speed of sound c_0 (sound propagation in an infinite fluid) and the effective speed of sound c in a channel with compliant walls.

$$c = \frac{c_0}{\sqrt{1 + B\gamma}} \tag{1}$$

The compliance of the tube, γ, represents the relative change of the tube cross sectional area when a unitary pressure is applied on the inner surface of the tube. B represents the bulk modulus of elasticity of the fluid, $B = \rho c_0^2$. As can be observed from Eq. 1, the effective speed of sound is smaller than the intrinsic speed of sound. This effect is increasing with the increase in the tube compliance.

The fundamental resonance frequency in a pipe with both ends open can be determined as

$$f_r = c/(2l') \tag{2}$$

where l' is the length corrected for end effects. The corrected length can be determined for open–open pipes based on the formulas given by Rossing[12] and Pierce[13]

$$l' = l + 0.61\,d \tag{3}$$

In case of circular cross section d represents the diameter, while for rectangular cross section we will take d as the smallest dimension of the rectangle.

For an open–closed pipe, Eq. 2 becomes

$$f_r = c/(4l') \tag{4}$$

with no corrections applied to the closed end.

If the fundamental resonance frequency can be determined, Eqs. 2 and 4 provide the means to determine the effective speed of sound within the fluid channels. Antohe and Wallace[14] showed that the resonance frequency can be determined with an impedance amplifier using the coupling between the electrical circuit defined by the piezoelectric element, in their case an annulus polarized along the radius, and the fluid inside the channel. The same principle can be applied to the channel configuration considered for this study.

We have used both methods (resonance measurement through the fluid/structure coupling and compliance determination) to determine the acoustic properties of the print head developed for Compaq.[8–10] The analysis looks at the effect of the channel length and boundary conditions (end effects produced by the supply manifold and the orifice plate) in terms of the resonance frequency/period.

Experimental Procedure

Print Head Configuration and Operation

The printhead analyzed consists of a series of channels that are sawn in a piezoelectric block assembled from a thin piece piezoelectric material bonded to a thicker base piece. Both pieces are poled along a direction perpendicular to the fluid channel. An orifice plate is bonded at the outlet of the channels, and fluid is supplied to a manifold at the back of the printhead. The supply manifold was tilted 51° with respect to the fluid channels, thus creating a printhead with channels of different lengths. In these experiments, the channel is 360 µm deep and 85 µm wide. A total of 121 channels are sawn across the printhead. The orifice diameter is 45 µm.

Figure 1 presents the actuating structure (left) and a cross section through a fluid channel (right). To create a drop an electrical signal is applied to the bond layer between the base and the thin piece on one wall with the mirror signal on the bond of the opposite wall while the top is held at 0 V. The resulting electrical fields produce the "instantaneous" deformation of the piezoelectric structure which is coupled to the fluid, thus generating acoustic waves that propagate along the channels. The motion of the piezoelectric structure is considered infinite because its lowest resonance frequency is two orders of magnitude greater than the fluid resonance resonant frequency.

The motion of the piezoelectric structure is described by a set of coupled equations. When the piezoelectric equations are written with the polarization direction being along the third axis, the properties of the piezoelectric material are as follows:

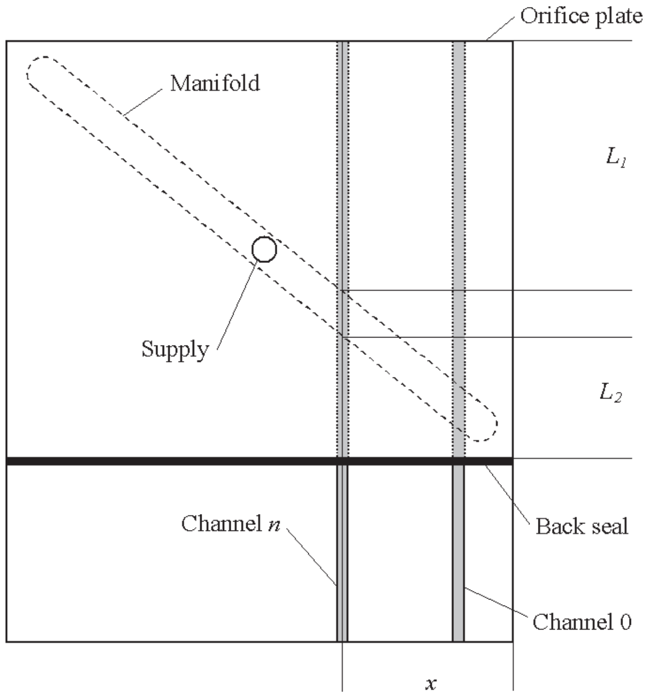

Figure 2. Length of printhead channels.

$$\mathbf{s} = \begin{bmatrix} 15.9 & -4.61 & -8.16 & 0 & 0 & 0 \\ -4.61 & 15.9 & -8.16 & 0 & 0 & 0 \\ -8.16 & -8.16 & 20 & 0 & 0 & 0 \\ 0 & 0 & 0 & 41.9 & 0 & 0 \\ 0 & 0 & 0 & 0 & 41.9 & 0 \\ 0 & 0 & 0 & 0 & 0 & 41.02 \end{bmatrix} \times 10^{-12} \ \mathrm{m^2/N}$$

$$\mathbf{d} = \begin{bmatrix} 0 & 0 & 0 & 0 & 690 & 0 \\ 0 & 0 & 0 & 690 & 0 & 0 \\ -283 & -283 & 552 & 0 & 0 & 0 \end{bmatrix} \times 10^{-12} \ \mathrm{m/V} \qquad (5)$$

$$\varepsilon = \begin{bmatrix} 1.55 & 0 & 0 \\ 0 & 1.55 & 0 \\ 0 & 0 & 1.25 \end{bmatrix} \times 10^{-8}$$

where ***s*** represents the elastic compliance matrix at constant electric field, ***d*** is the piezoelectric constant matrix (strain/field at constant stress), and **e** is the relative dielectric constant with respect to free space

$$(\varepsilon_0 = 8.85 \times 10^{-12} \text{ F/m}).^{15}$$

For acoustical purposes the channel is defined lengthwise by the orifice plate at one end and the supply manifold at the other end. When data are collected without the orifice plate or the back seal, the constant (atmospheric) pressure at that boundary determines the acoustical termination of the channel. The printhead used in this work had a slanted manifold (Fig. 2). The manifold separates the channel in a front part of decreasing length L_1 and a back part of increasing length L_2 for increasing channel number. Figure 3 depicts the length variation for the front and back portion of the channel as a function of channel number. Drops are generated by the front part of the channel but acoustic resonance is detected for both regions.

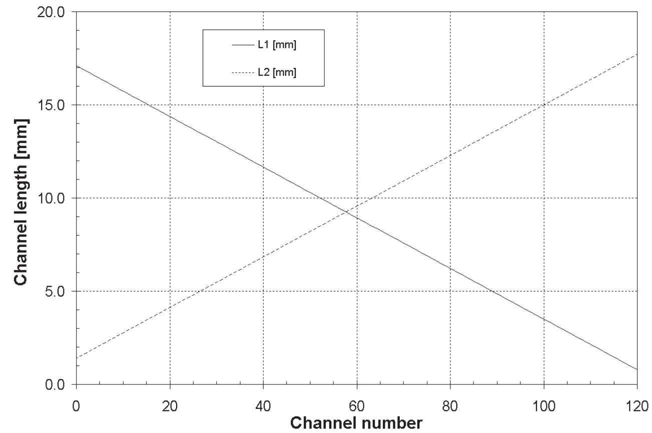

Figure 3. Front and back channel length values as functions of channel number.

Measurement of the Acoustical Resonance Frequency

An HP4149A impedance amplifier was used to analyze the impedance variation for several frequencies.[14] The electrical impedance analyzer is connected to the electrodes at the middle of the tooth. The results of the logarithmic frequency sweep, performed for the from 10 kHz to 200 KHz with the printhead filled with isopropyl alcohol (IPA), were transferred from the impedance analyzer to a computer through a GEPIB interface using a program written in Quick Basic. A total of 400 points were acquired in the range of interest (10 kHz to 200 kHz) for each frequency sweep. The acoustical resonance frequencies for the filled printhead appear as additional (besides the structural resonance frequencies—present also on a non-filled printhead) peaks in the impedance curve. For this specific configuration two acoustic resonance peaks appear, one for each part of the channel.

Determination of the Channel Compliance

The compliance was determined using ANSYS, a finite element program with piezoelectric capability. A transformation of the matrices containing the piezoelectric properties presented in Eq. (5) was necessary as ANSYS requires direction 1 to be the polarization direction. A two dimensional cross section of the print head was modeled in ANSYS using plane stress elements (free movement along the direction perpendicular to the cross section). The model consisted of half of the analyzed channel and half of the neighboring channel. The neighboring channel was filled with fluid while the analyzed channel was empty. A boundary condition of zero voltage was set at the two electrode layers with a pressure of 1 kPa on the inner surface of the channel of interest.

Figure 4 presents the deformed structure from an ANSYS run. The compliance was determined by integrating the displacement along the circumference of the channel and found to be to be $\gamma = 5.81 \times 10^{-10}$ Pa^{-1}.

Results and Discussions

Acoustic Resonance Measurements

From an acoustical perspective the two parts of the channels are independent resonant pipes with the manifold providing an open end condition for both. Measurement of the acoustic resonance in the channels was done for different stages of the printhead construction:

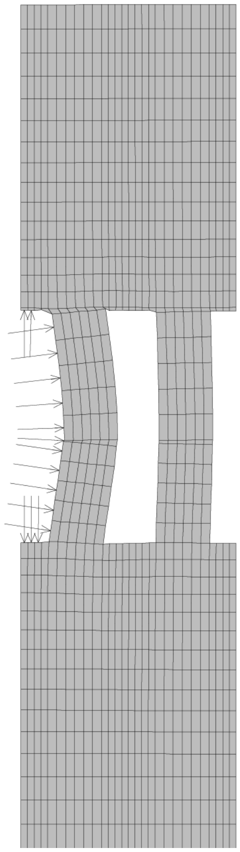

Figure 4. ANSYS finite element model deformed structure used for channel compliance determination.

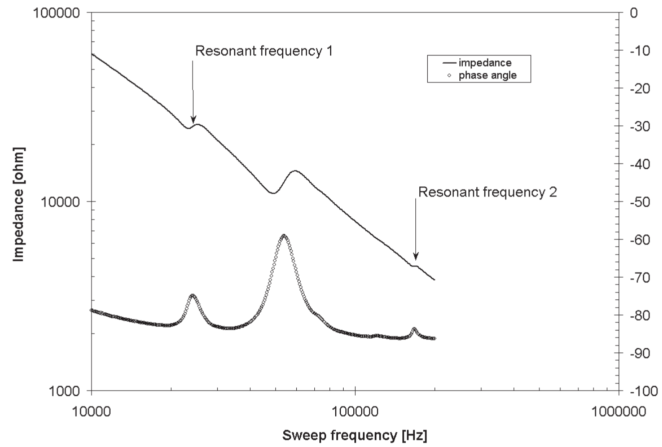

Figure 5. Frequency sweep - impedance and phase angle.

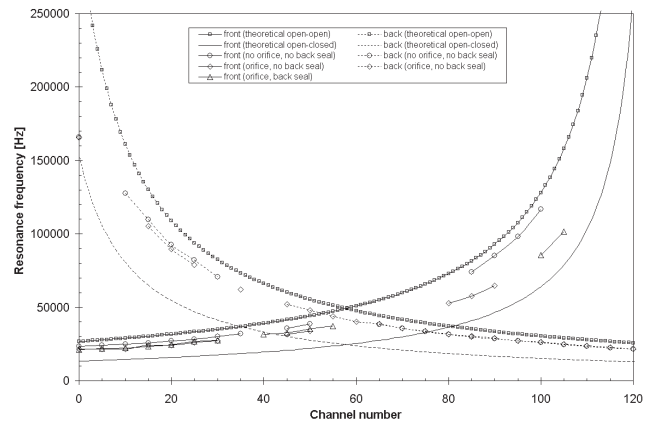

Figure 6. Comparison of resonant acoustic frequencies for different boundary conditions.

printhead without orifice plate and back seal, with orifice plate and without back seal, and with orifice plate and back seal.

A frequency sweep with the electrical impedance analyzer connected to the bond areas at the middle of the channel walls shows the acoustic resonance frequency in both parts of the channel. A typical result for a channel filled with isopropyl alcohol is presented in Fig. 5.

On both the phase angle and the impedance curves we can observe three locations that exhibit resonance characteristics. The middle one corresponds to a mechanical structure resonance (detected for frequency sweep with the non-filled printhead) that does not interfere with the fluid/actuator coupling, while the other two are produced by the acoustic resonance in the two parts of the fluid channel: resonant frequency 1 corresponds to the longer part of the channel and resonant frequency 2 corresponds to the shorter part. A sequence of plots from channel 0 to 120 would show the resonant frequency generated by the front part of the channel moving towards the right (increasing), passing the structural resonant frequency and continuing to move towards the right as the length of the front part reduces. The resonant frequency generated by the front part moves in the opposite direction (increasing length).

Figure 6 presents a summary of the acoustic resonant frequencies measured for various boundary conditions. The theoretical curves use Eqs. 2 and 4 for the front and back part of the channel respectively. The compliance value (5.81×10^{-10} Pa^{-1}) determined from the ANSYS structural analysis and the measured lengths corrected using the channel width as the characteristic dimension were used to compute the results presented in Fig. 6.

The dotted lines correspond to the back part of the channels and the solid lines to the front of the channel. The curves are also identified by the instance in the fabrication process when data was collected. Very little differences are observed in the resonant frequency for the back part of the channel with and without orifice plate. The resonance peak was no longer observed for the back part of the channel after back seal. The back part of the channel had a dead end at the back seal and air was trapped in that region when filling the channel. This air pocket most likely absorbed all the acoustic reflections that were no longer transmitted to the peizoelectric structure, thus not shown by the electrical impedance measurement. Resonance frequency values are closer to the open–open theoretical curve than to the open–closed one.

For the front part of the channels, the frequencies without orifice and no back seal are even closer to the theoretical open–open curve, compared to the back part of the channel. This is most likely because the end of

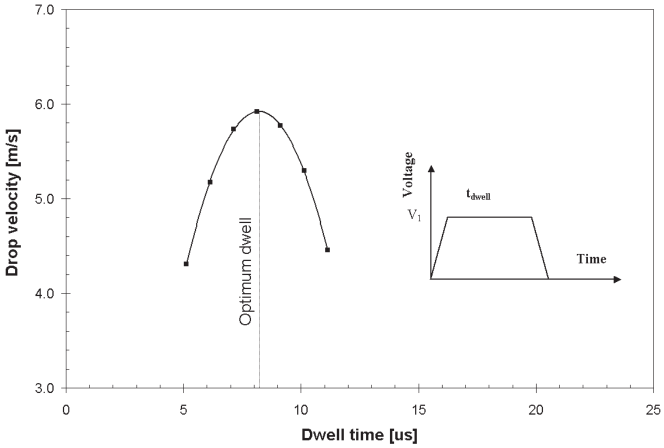

Figure 7. Drop velocity as a function of dwell time—channel 79; drive pulse parameters.

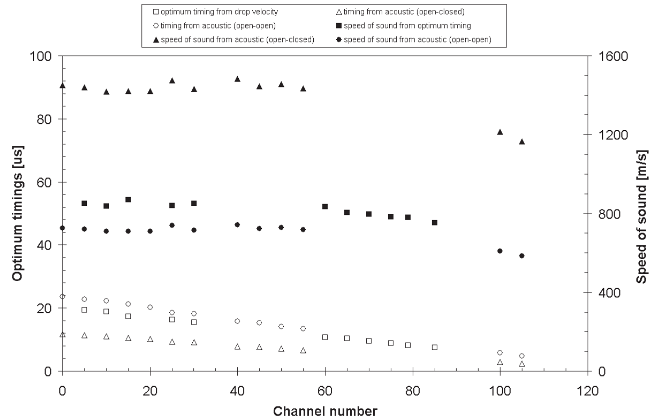

Figure 8. Optimum dwell time and speed of sound.

the back part of the channel where the seal is applied continues with the channel in the base even when not back sealed, so is not truly open. A larger length correction should be used for the open end of the back part of the channel. After the orifice plate is mounted the resonant frequency shifts towards the theoretical open–closed curve. The theory for organ pipe resonances,[12] being the solution to an eigenvalue problem, allows only for a discontinuous jump in resonant frequency as the terminal impedance changes.

Timings for Optimum Driving Conditions

The functional characterization of the printhead was performed with isopropyl alcohol at 60 Hz. Actuation of the piezoelectric structure was done with a trapezoidal waveform as presented in Fig. 7. The time at high voltage (dwell time) is measured for practical purposes between the middle of the two transition periods. The increasing ramp of the trapezoidal corresponds to an expansion of the channel cross section with the decreasing ramp corresponding to a decrease in channel cross section. During the expansion a negative pressure wave travels to the supply end where it reflects as a positive pressure wave.

The optimum timing is defined as the dwell time for which a maximum velocity is achieved for a constant applied voltage. Based on the wave propagation in the channel (the fall should reinforce the high pressure wave reflected from the supply manifold) the optimum timing is determined from the time it takes the wave to travel to the supply end and back

$$t_{opt} = l'/c \tag{6}$$

In the formula l' is the corrected length of the channel and c is the effective speed of sound in the channel. Figure 7 presents the drop velocity as a function of the dwell time. When the fall from high voltage to zero voltage occurs before or after the reflected waveform reaches the middle of the channel some cancellation occurs resulting in a loss of energy. The optimum dwell time is determined by the maximum in the drop velocity curve presented in Fig. 7. It is important to note that the reduction in channel length results in a smaller drop size, thus being a tool to generate smaller drops with the same orifice diameter.[7,16] Another advantage of a reduced channel length is the ability to increase the operating frequency.

Figure 8 shows the optimum timing and the speed of sound as a function of channel number, linear with the channel length. The filled symbols refer to the speed of sound in the channel and the unfilled symbols describe the optimum dwell time. Optimum dwell time derived from drop velocity measurements (square) is used to derive the effective speed of sound (filled square) from Eq. 6.

The acoustic resonant frequency from the electrical impedance measurement of the front part of the channel (with orifice plate) is used in Eqs. 2 and 4 to determine the speed of sound in the channels assuming an open–open and an open–closed pipe, respectively. The two values for the speed of sound are used in Eq. 6 to determine the corresponding optimum dwell time (triangular symbol for open–closed and circular symbol for open–open).

From this comparison we can conclude that the channels of an operational printhead behave from an acoustical perspective more like an open–open tube.

Conclusions

Electrical impedance measurements were used to evaluate printhead acoustics and showed that fluid channels in an ink jet printhead do not behave as an open–closed tube. The same behavior was identified from the optimum timings for the driving waveform. This could be a result of the presence of the orifice and of the compliance of the orifice plate itself.

This study shows that the optimum timing of the driving waveform can be reasonably approximated using the effective speed of sound derived from the acoustic resonant frequencies (impedance measurements). Another option is to use the speed of sound derived using the channel compliance and the speed of sound of the infinite fluid. Both ways lead to slightly longer than optimum dwell time values.

Experimental results showed that by reducing the channel length the optimum waveform duration decreases allowing operation at higher frequencies. Another advantage of shorter channels consists in the ability to generate drops with a smaller diameter than the orifice diameter.

Glossary

A = area of the open cross section of the fluid channel [m^2]
B = bulk modulus of elasticity of the liquid [Pa]
c_0 = speed of sound as intrinsic property of the liquid [m/s]
c = effective speed of sound in the fluid channel [m/s]
d = piezoelectric constant matrix: strain/field at constant stress [m/V]
f = frequency [Hz]
l = length of the channel [m]
l' = corrected length of the piezoelectric transducer due to end effects [m]
s = elastic compliance matrix at constant electric field [m^2/N]
t = time [s]
ε = relative dielectric constant – clamped
ε_0 = dielectric constant of the free space [F/m]
γ = compliance of the channel [Pa^{-1}]
ρ = density of the liquid [kg/m^3]

References

1. Lord Rayleigh, *Proc. Lond. Math. Soc.* **10,** 4 (1879).
2. E. F. Goedde and M. C. Yuen, *J. Fluid Mech.* **40**: 495 (1970).
3. A. H. East, U.S. Patent 5,561,452 (1996).
4. J. A. Katerberg and D. N. Pipkorn, U.S. Patent 4,972,201 (1990).
5. J. F. Dijksman, *J. Fluid Mech.* **139,** 173 (1984).
6. D. B. Bogy and F. E. Talke, *IBM J. Res. Develop.* **28,** 314 (1984).
7. D. B. Wallace, V. Shah, D. J. Hayes, and M. E. Grove, *J. Imaging Sci. and Tech.* **42**, 390 (1996).
8. J. R. Pies, D. B. Wallace and D. J. Hayes, U.S. Patent 5,235,352 (1993).
9. J. R. Pies, D. B. Wallace and D. J. Hayes, U.S. Patent 5,433,809 (1995).
10. J. R. Pies, D. B. Wallace and D. J. Hayes, U.S. Patent 5,554,247 (1996).
11. B. E. Wylie and V. L. Streeter, *Fluid Transients in Systems*, Prentice Hall, Englewoods Cliffs, NJ, 1993, p. 5.
12. T. D. Rossing, *The Science of Sound*, Addison-Wesley Publishing Company, Boston, MA, 1982, p. 53.
13. A. D. Pierce, *Acoustics. An Introduction to Its Physical Principles and Applications*, McGraw-Hill, New York, 1981, p. 348.
14. B. V. Antohe and D. B. Wallace, *J. Meas. Sci. Tech.* **10,** 994 (1999).
15. Morgan Matroc Inc. *Piezoelectric Technology. Data for Designers (Morgan Matroc Inc., Electro Ceramic Division).*
16. D. B. Wallace and J. L. Stortz, U.S. Patent 5,461,403 (1995).